IEEE Access
Multidisciplinary ⋮ Rapid Review ⋮ Open Access Journal

Received 5 July 2023, accepted 27 July 2023, date of publication 1 August 2023, date of current version 11 August 2023.

Digital Object Identifier 10.1109/ACCESS.2023.3300726

RESEARCH ARTICLE

Deep Learning-Based Fall Detection Using WiFi Channel State Information

YI CHU[1], KANAPATHIPPILLAI CUMANAN[1], (Senior Member, IEEE), SATHISH K. SANKARPANDI[2], STEPHEN SMITH[1], (Member, IEEE), AND OCTAVIA A. DOBRE[3], (Fellow, IEEE)

[1]School of Physics, Engineering and Technology, University of York, YO10 5DD York, U.K.
[2]Yaanai Ltd., IP3 9UN Ipswich, U.K.
[3]Faculty of Engineering and Applied Science, Memorial University, St. John's, NL A1C 5S7, Canada

Corresponding author: Yi Chu (yi.chu@york.ac.uk)

This work was supported by the Engineering and Physical Sciences Research Council (EPSRC), U.K., under Grant EP/R51181X/1.

ABSTRACT Falls have always been one of the major threats to the health and well-being of elderly people, particularly for those living alone. Both wearable and non-wearable fall detection systems have already been developed. However, the fall detection systems using WiFi channel state information (CSI) have attracted a significant interest from researchers due to their non-intrusive and low-cost nature. There are existing machine learning (ML) based fall detection systems using WiFi CSI; however, most systems trained with comprehensive datasets tend to achieve relatively lower accuracy compared to that of the systems trained with less inclusive datasets. To address these issues, we propose a novel, deep learning based fall detection technique. First, we implement different WiFi CSI collection tools and evaluate their potential for fall detection. To develop a highly accurate fall detection technique, we construct a comprehensive dataset, which consists of over 700 CSI samples including different types of falls and other daily activities, performed in four different indoor environments on and off the dominant paths. With this dataset, we then develop a deep learning based classifier using an image classification algorithm. The proposed technique, unlike the other fall detection systems, only requires down sampling and reshaping in pre-processing. The proposed fall detection system is evaluated with the constructed dataset, and it outperforms two other existing systems. It achieves over 96% accuracy for CSI collected in all four environments and 99% accuracy for CSI collected in certain combinations of the environments.

INDEX TERMS Fall detection, deep neural networks, WiFi sensing.

I. INTRODUCTION

According to the Office for National Statistics (ONS), the UK population over 65s has been steadily growing and it is estimated to rise by another two million by 2025 [1]. In this age group, falls are the most common cause of hospitalisation, and they sometimes even lead to death. Over half the falls are critical to the mobility of the older adults and most victims are immobilised for an hour or more after a fall and unable to call for help [2]. In the US, about 40% of the old age group living at home will fall at least once each year, and about 2.5% of them will be hospitalised [3]. Falls are also major causes of disability and reduced independence in older people. In the UK, accidental falls have contributed 29% of disability in people aged 65 years or older, and 32% in those aged 75 years or older [4]. Fear of falling and a lack of access to help after a fall are causes of distress, loss of confidence, independence, and mortality in older adults. Therefore, an efficient fall detection system is of paramount importance to both the physical and mental health of older adults.

Given the significance of fall detection, several technologies have already been developed. For wearable technologies, a range of devices are used in the form of small gadgets such as a watch and a sticky patch [5]. These devices, in general, monitor the posture of the wearer by analysing the data from

The associate editor coordinating the review of this manuscript and approving it for publication was Chuan Li.

their sensors (e.g., gyroscope and accelerometer) and detect fall events. In addition, there are fall detection systems developed for smartphones, given that most modern smartphones have a wide range of sensors integrated [6]. Wearable systems are mostly effective and accurate; however, due to requiring attachment to the body and frequent battery changes, they are less popular with older adults. For the non-wearable technologies, vision-based methods play a key role in detecting falls using data collected by sensors such as RGB cameras and infrared cameras [7], [8], [9]. Vision-based systems offer the highest accuracy. However, the coverage area is usually limited by the field of view of the sensors and the invasive nature of the vision-based monitoring may not be comfortable for all older adults, and the privacy issues come along with this type of monitoring.

Based on the above challenges and our initial discussions with older adults from Parkinson's UK with a history of falls, we concluded that the fall detection system should be non-intrusive and accurate. To meet these requirements, fall detection systems using wireless signals (e.g., WiFi signals) are suitable candidates for the task given the non-intrusive, ubiquitous, and low-cost advantages of the WiFi-based systems. WiFi-based human sensing applications emerged when WiFi networks were just becoming commonly used across the world. For example, the localisation application [10] uses WiFi received signal strength indicator (RSSI) to track the human presence. However, the performance of RSSI-based systems is naturally limited due to single measurement of the received signal power, which could be affected by many external factors such as propagation distance and obstacles on the path.

Orthogonal frequency division multiplexing (OFDM) based IEEE 802.11a/g/n/ac devices use multiple subcarriers and multiple antennas to compensate for the effect of frequency selective fading [11]. The channel state information (CSI) available at the WiFi receiver provides detailed amplitude and phase information of individual subcarriers. With this information, CSI offers a much better frequency resolution than RSSI, therefore, becoming a more promising tool for wireless sensing tasks [12].

A. RELATED WORKS

A number of studies [13], [14], [15], [16], [17] have already investigated fall detection techniques using WiFi CSI. These techniques usually involve 3-step operations to detect falls: (1) CSI data pre-processing which involves operations such as resampling, filtering, and principal component analysis (PCA) [18]; (2) CSI feature extraction which highlights data of interest by observing features such as CSI spectrogram, normalised standard deviation, entropy, and power decline ratio; (3) event classification which identifies whether the collected CSI involves fall or non-fall events using classifiers based on support-vector machine (SVM), convolutional neural network (CNN) or long short-term memory (LSTM). However, the detection accuracy of these techniques mostly depends on the dataset used for training. For example, FallDeFi [14] provides a dataset with hundreds of falls and daily activities in several environments and achieves a maximum of 88.9% accuracy. The work in [15] reports 100% accuracy with the dataset of only 80 falls performed in a single-room environment.

ResFi performs indoor localisation with CSI data using a ResNet based structure but replacing residual blocks with stochastic residual blocks [19]. Chen et al. propose an attention based bidirectional LSTM [20] system which uses CSI data to identify different types of daily human activities including walking, running, sitting down and standing up. Yousefi et al [16] propose a human behaviour recognition system which uses LSTM and recurrent neural network (RNN) to identify six different activities including falls. Wang et al. [21] propose a 1-D ResNet classifier to detect six different hand activities and to provide indoor localisation with CSI data. E2EDLF [22] recognises activities involving interactions between two humans (such as handshaking, hugging and high fiving) using CSI data with a CNN based system. Li et al. [23] compare the capabilities of CSI and WiFi radar-based sensing applications and discuss the performance differences in LoS and NLoS conditions.

WiFall [24] and RT-Fall [17] are the early work which build the steppingstones of fall detection using CSI data. Both approaches use an SVM-based classifier to detect fall events. FallDeFi [14] improves the performance of WiFall and RT-Fall by extracting features by applying short-time fourier transform (STFT) spectrogram and power burst curve (PBC). FallDeFi has included several non-fall daily activities, which have similar features to falls (e.g., sitting down and picking up objects) to reduce false alarms and achieve a maximum of 88.9% accuracy under certain conditions. Damodaran et al. propose a CSI-based fall detection system [15] with a classifier combing both SVM and LSTM. This system achieves 100% accuracy in fall detection however the dataset is collected in a single-room environment and the sample size of fall events is relatively small (80 samples). Nakamura et al. [25] propose a fall detection system using spectrogram images generated from CSI data to recognise fall events. The spectrogram images are used as input to a ResNet based image classifier to identify falls. The proposed work achieves a maximum of 96% accuracy in certain environments. However, similar to the work in [15], the CSI data is collected in a limited number of environments (two small rooms with WiFi modules placed close to each other for LoS propagation).

There are a number of works that achieve remarkable accuracy but have similar limitations. For example, Mattela et al. [26] report a maximum of 99% accuracy from the proposed LSTM-based classifier but the dataset only includes CSI collected in two environments and the recorded non-fall activities only include walking and sitting up. Hu [27] propose a method to detect falls by estimating the speed and acceleration of moving objects using CSI. The works achieves a maximum 95% detection rate with a dataset

including three indoor environments. However, as pointed out by the authors, the work focuses on hard falls and the detection rate reduces with lower-speed falls.

From the above reviews, the existing work tends to report a relatively lower accuracy while having a comprehensive dataset (e.g., FallDeFi [14]) or a remarkable accuracy but with a limited dataset (e.g., the work in [15]). Comparison of the proposed datasets are provided in Table 1. These results confirm that a fall detection system which remains accurate across different environments and identifies falls from other daily activities is needed. Therefore, in this paper, we construct a comprehensive WiFi CSI data set and propose a novel deep learning based fall detection technique using the dataset.

B. CONTRIBUTIONS

With the comprehensive WiFi CSI data set, we develop a deep learning classifier based on a state-of-the-art image classification algorithm [28] to accurately identify fall events and to reduce the pre-processing. Our contributions are summarised as below.

- We implement various existing WiFi CSI collection methods to evaluate and compare their potentials for fall detection applications. Although WiFi devices are well standardised and widely used in homes, not all devices are suitable for fall detection applications. Our experiments show that the collected CSI has varying qualities when different commercial off-the-shelf WiFi devices were used. It is important to review the capability of the hardware when developing the fall detection for real-world applications.
- To develop a highly accurate WiFi sensing based fall detection technique, we create a comprehensive WiFi CSI dataset which includes falls and other daily activities performed in four different indoor environments. Events that occurred on and off the dominant paths are included in the dataset to improve the detection performance in practical scenarios. We recruited twenty-two volunteers (ages 24 to 43, 7 females and 15 males) and performed over 700 controlled falls and other daily activities in four different indoor environments to collect CSI data with different propagation conditions including Line-of-Sight (LoS), Non-Line-of-Sight (NLoS), on and off dominant propagation path.
- We propose a novel deep learning based falls detection technique, using WiFi CSI. The proposed technique is evaluated against two other fall detection systems ([14] and [25]) and it outperforms both systems in all experiment scenarios. In particular, it achieves over 96% detection accuracy when using the collected CSI data in all environments and 99% accuracy when using certain subsets of the collected CSI data. It also achieves over 97% accuracy while testing with the dataset collected in three different indoor environments with LoS and remains over 92% when the propagation conditions become more complex.
- The size and sample variety of the training dataset have great impact to the performance of deep learning based classification. Unlike image classification, preparing and expanding large datasets for fall detection is much more difficult and requires contribution of the research community. Therefore, we made our work available in the public domain[1] so the readers interested in further tuning or implementing the proposed fall detection technique could easily expand or replace our dataset to improve the detection performance.

The rest of the paper is organised as follows. The state-of-the-art of CSI collection methods and the details of evaluation and comparison across available CSI collection tools are presented in Section II. The background of deep learning based classification and workflow of the proposed fall detection are explained in Section III. The CSI data collection in different environments and dataset construction are presented in Section IV. The classification performance results are presented in Section V with discussions on its advantages and limitations. Section VI concludes the paper.

II. WIFI CSI COLLECTION TOOLS

Designing a WiFi CSI-based fall detection system not only requires accurate classification but also reliable CSI collection with low-cost equipment. Although CSI plays a key role in IEEE 802.11n (and beyond) WiFi systems [29], very few commercially off-the-shelf WiFi devices allow the CSI to be extracted. In this section, we review different CSI collection tools and evaluate their potential for fall detection.

At the moment, commonly used WiFi CSI extraction methods include:

- Linux 802.11n CSI Tool [30] which extracts CSI from the Intel 5300 NIC chipset with custom firmware
- Atheros CSI Tool [31] which extracts CSI from Atheros 9K WiFi chipsets with modified firmware
- ESP32 [32] based tools such as ESP32 CSI Toolkit [33] and Wi-ESP [34] which use the lightweight ESP32 based WiFi transceiver modules to collect CSI
- Nexmon CSI extractor [35] which extracts CSI from certain Broadcom WiFi chips

The Linux 802.11n CSI Tool [30] can extract CSI from the Intel 5300 NIC chipset and the Atheros CSI Tool [31] can extract CSI from Atheros 9K chipsets. For a 20 MHz channel, Intel 5300 NIC chipset provides the in-phase and quadrature (IQ) of 30 (out of 64) subcarriers with an 8-bit resolution and Atheros 9K series chipsets provide the IQ of 56 subcarriers with a 10-bit resolution. Both types of chipsets support CSI extraction on 2.4 GHz and 5 GHz WiFi bands, 20 MHz and 40 MHz channels, and up to 3 antenna elements. The tools for both chipsets allow frequent CSI packet transmission and reception. For the Atheros CSI Tool, a maximum of 4K CSI packets can be transmitted per second, and for the Linux 802.11n CSI Tool 1K CSI packets per second are commonly used by researchers (maximum rate is not mentioned in particular). To use these tools, a compatible computer with

[1] https://github.com/yc541/ENetFall

TABLE 1. Comparison of the existing datasets.

Dataset	Falls/other activities	Environments	Activity types	Participants	LoS/NLoS	Publicly available
FalldeFi [14]	326/744	5	11	Unknown	Both	Y
Work in [15]	80/420	1	4	Unknown	LoS	N
Work in [16]	120/600	1	6	6	LoS	Y
Work in [17]	1200/1200	4	8	6	Both	N
Work in [25]	Unknown	2	10	Unknown	LoS	N
Work in [24]	2850/8500	3	4	19	Both	N
Work in [26]	Unknown/775	2	5	Unknown	LoS	N
Work in [27]	846/814	3	4	10	Both	N
Proposed work	321/436	4	8	22	Both	Y

at least one available Mini-PCIe slot is essential. One constraint of using these tools is sourcing a compatible computer because both chipsets were initially released before 2010 and it is unlikely for new computers to be compatible with these chipsets.

The Nexmon CSI extractor [35] uses modified firmware to extract CSI from a range of Broadcom WiFi. This tool supports both 2.4 GHz and 5 GHz frequency bands with up to 80 MHz bandwidth and extracts the amplitude of up to 256 subcarriers. Nexmon requires a rooted Nexus 5 or 6P smartphone, or a Raspberry Pi B3+/B4 or an Asus RT-AC86U WiFi router to be used as the CSI extractor (with WiFi monitor mode) to overhear CSI packets exchanged between a commercial WiFi access point (AP) and a WiFi client (e.g., a mini-PC or laptop). Compared to the Linux 802.11n and the Atheros CSI Tools, the hardware required by Nexmon is easier to source. However, the amount of preparation for the CSI extraction is similar.

The other widely used CSI collection hardware is the ESP32-based Internet of Things (IoT) WiFi module. There are many WiFi modules developed based on ESP32 with assorted brands available in the market, and they all share the same features of small size, lightweight and low power consumption. For example, the TTGO T8 module [36] only has the dimension of 6.5 $\times$ 2.5 cm, weighs 7 grams, and can be powered by a 5 V USB. It also has a microSD card slot which allows CSI data to be stored. The ESP32-based modules support a 2.4 GHz WiFi band, 20 MHz and 40 MHz channels, and one antenna. Unlike the PCIe WiFi chipsets, the ESP32-based modules can be used independently from computers (unless configuring the modules) which makes the deployment significantly easier. However, due to the limitations of the processing power of the board, the CSI acquisition rate is less than 200 packets per second according to our tests.

The accuracy of a fall detection system is not only determined by the capability of the classifier but also relies on the quality of the collected CSI. In the following subsections, we review the details of three different CSI collection methods and compare their suitability for the fall detection tasks.

A. CSI COLLECTION USING ESP32 BASED IoT MODULES

The advantages of the ESP32 based CSI collection tools are their small form factors and the capability to operate without host computers. The issues which limit their applicability are the WiFi bands (2.4 GHz only), low CSI sampling frequency (less than 200 Hz) and a single antenna. According to the measurements made by Kroonenberg, et al. [37], the typical velocity of a falling adult (from standing) ranges from about 2 m/s to 3.5 m/s immediately before impact to the mattress. The Doppler frequency of a falling adult can be calculated using the Doppler frequency equation,

$$f = \frac{2v}{\lambda}, \tag{1}$$

where f denotes the Doppler Frequency, v denotes the velocity of the falling adult and λ denotes the wavelength. For the 2.4 GHz WiFi signals $f \in [32, 56]$ Hz, and for the 5.2 GHz WiFi signals $f \in [69, 121]$ Hz. Since the velocity of the falling adult is less than the velocity before impact during most of the fall interval, the Doppler Frequency of the whole fall duration would result in a lower range. As pointed out in [14], the strongest signal energy of high-frequency activities is concentrated at the Doppler Frequency of below 30 Hz for the 5.2 GHz WiFi signals (or 14 Hz for 2.4 GHz WiFi signals). The lower Doppler Frequency of the target activities at 2.4 GHz makes it less distinguishable from the noise floor, therefore increasing the difficulty for detection and making 2.4 GHz less suitable for fall detection systems. In this section, we demonstrate our experiments using two different types of ESP32 based WiFi modules and review their capability for fall detection.

We first use a pair of NodeMCU modules, with one set to AP mode (transmitter) and the other set to client mode (receiver). The two modules are placed about four metres away with a LoS path, and the CSI packet rate is set to 200 packets/s. Fig. 1 shows a two-second section (400 CSI packets) of the CSI collected while there is no activity in the room. Fig. 1(a). shows the CSI collected for all subcarriers. It can be observed that there are frequent random amplitude spikes and fluctuations that occur across all subcarriers. To extract useful features from this CSI some preprocessing is required otherwise these fluctuations will result in a significant amount of high frequency noise. Fig. 1(b). shows the raw and pre-processed amplitude of subcarrier 10. A sliding window of 200 CSI packets is implemented to compute the average amplitude within one second. If a certain amplitude exceeds 1.5 times the average amplitude, it is then

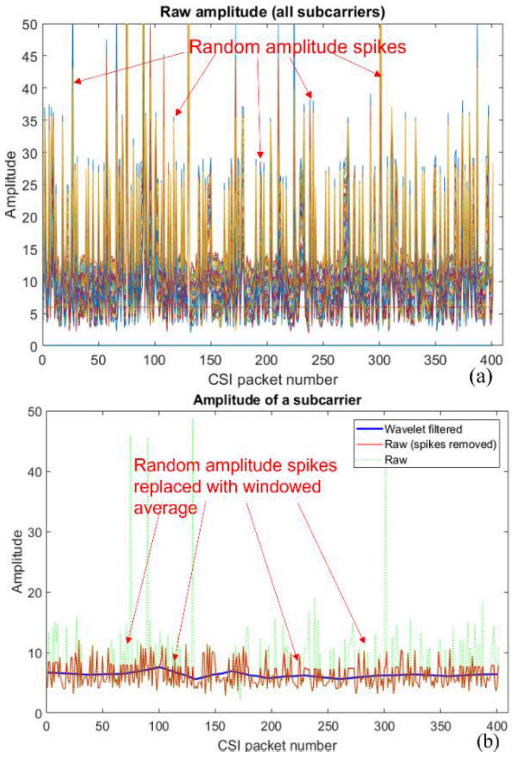

FIGURE 1. CSI amplitude collected by NodeMCU modules. (a) CSI of all subcarriers. (b) CSI of subcarrier 10.

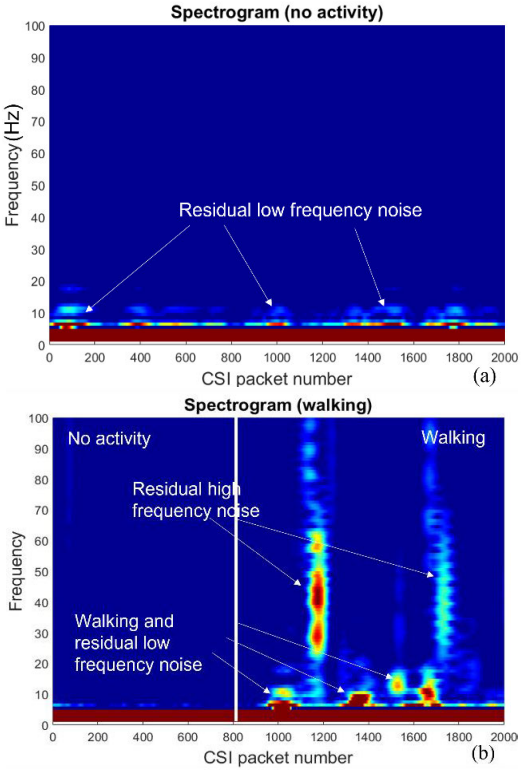

FIGURE 2. Spectrograms for (a) No activity, and (b) Walking of CSI from NodeMCU.

replaced with the average amplitude. After the spike removal, a wavelet filter (the same as FallDefi [14], symlet wavelet function and 10 wavelet levels) is applied to remove the residual noise. As seen in Fig. 1 (b), there are still some fluctuations left after the wavelet filtering (a flat line is expected), which causes low frequency noise.

We then use Short-Time Fourier Transform (STFT) to observe the time-frequency features of the collected CSI in spectrograms to verify its quality. The sampling frequency of the spectrogram is set to 200 samples/s, the window size is set to 128, the number of overlapped samples is set to 110 and the Fast Fourier Transform (FFT) size is set to 128. This configuration results in a frequency resolution of 1.56 Hz and a time resolution of 90 ms. To generate the spectrograms, we use the CSI collected for all 52 WiFi data subcarriers (subcarriers 7 to 32, and 34 to 59). Fig. 2 presents the spectrograms generated from the CSI of two ten-second sections. In Fig. 2 (a), we can still observe residual low frequency noise at about 10 Hz and below even after the spike removal and wavelet filtering, where we should only see noise floor on the spectrogram when there is no activity in the room. In Fig. 2 (b), there is no activity in the room within the first nine seconds and the spectrogram is relatively clean. Once the activity starts (walking), we can observe signal energy above the noise floor. However, due to the residual low frequency noise observed in Fig. 2 (a), it is not straightforward to distinguish the signal energy caused by the walking activity from the residual noise because the signal energy rarely exceeds 20 Hz (close to noise frequency). There is also noticeable residual high frequency noise, which could potentially be removed by a low pass filter.

We also evaluate the CSI collection of a pair of TTGO T8 modules, in the same environment as the NodeMCU modules. Fig. 3 presents another four-second section of the collected CSI. Compared with the CSI collected by the NodeMCU modules, we observe few random spikes, however, amplitude fluctuations still exist after spike removal and wavelet filtering, resulting in residual low-frequency noise.

Fig. 4 depicts the spectrograms generated from the CSI of two ten-second sections collected by the TTGO T8 modules. Similar to Fig. 2, we can observe residual low frequency noise mostly below 15 Hz when there is no activity in the room. When there are activities in the room, we can observe signal energy at below 20 Hz. However, the feature of the activity is still not clearly distinguishable from the noise. We experience similar issues across multiple pairs of ESP32 based modules and the root causes are not clear. The issues could be caused by the build quality of the low-cost WiFi chips and (or) potential interference from other WiFi devices, which is mostly unavoidable in modern indoor residential environments. Therefore, we can conclude that the ESP32 based WiFi collection tools could potentially be viable for detecting the existence of activities but not for distinguishing of activities, including falls.

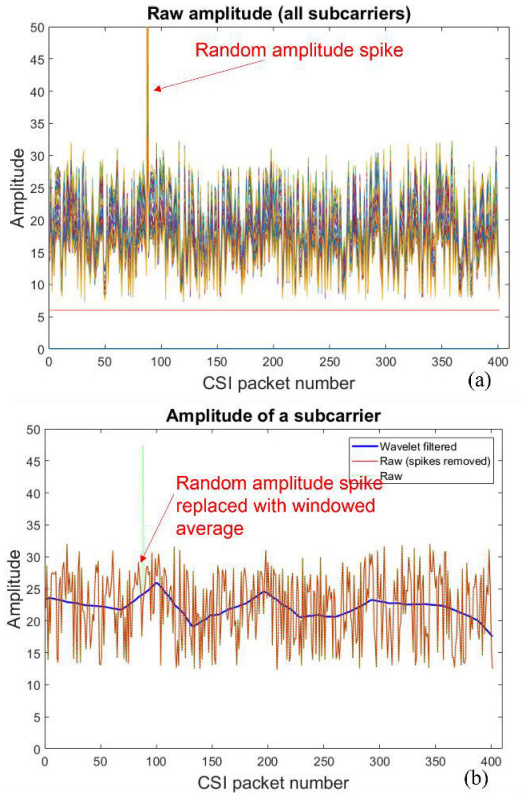

FIGURE 3. CSI amplitude collected by TTGO T8 modules. (a) CSI of all subcarriers. (b) CSI of subcarrier 10.

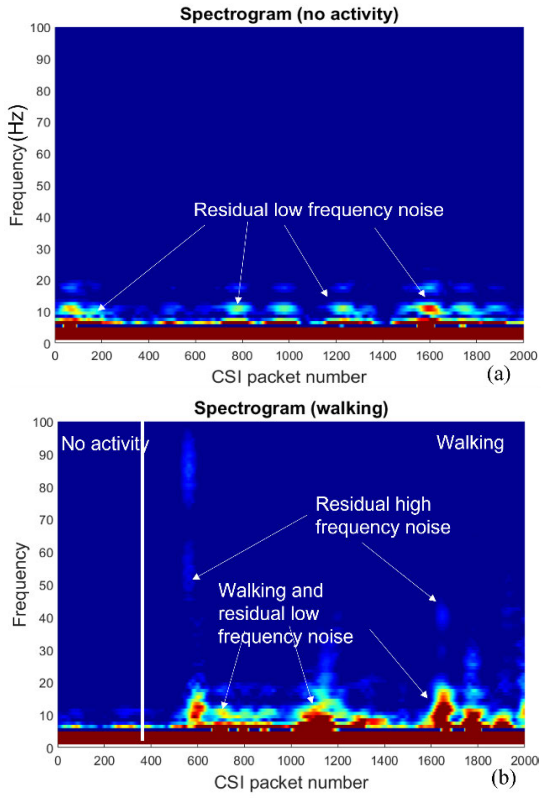

FIGURE 4. Spectrograms for (a) No activity, and (b) Walking of CSI from TTGO T8.

B. CSI COLLECTION USING INTEL 5300 NIC AND A COMMERCIAL AP

Compared with the ESP32 based CSI tools, the Intel 5300 NIC based CSI tool records CSI streams from multiple TX and RX antenna pairs, therefore improving the spatial diversity of the received signal. However, a compatible host computer is required to operate this CSI tool. In this paper, we use a Lenovo ThinkPad R61 (which was announced in 2007) with Ubuntu 14.04 LTS as the host computer. In Subsection II-A) the requirement of the 5.2 GHz WiFi band for fall detection tasks was established, therefore, in the rest of the paper, we use 5.2 GHz for CSI collection by default if the hardware supports it. Since this CSI tool supports a much larger sample rate, we set the CSI packet rate to 1000 packets/s. For the spectrogram observation, we set the sampling frequency to 1000 samples/s, the window size is set to 512, the number of overlapped samples is set to 256 and the FFT size is set to 256. This configuration results in a frequency resolution of 3.91 Hz and a time resolution of 256 msec. The maximum frequency of the spectrogram is set to 250 Hz since there is barely any signal energy beyond this frequency.

We first test this CSI collection tool with a Netgear WAC104 - AC1200 WiFi AP. Note that this CSI tool requires the client (laptop) to join the AP's WiFi network so the client can request CSI packets from the AP. With this combination, the CSI tool collects three CSI streams from one TX antenna and three RX antennas. Fig. 5 (a) illustrates a ten-second section of the wavelet filtered CSI amplitude when there is no activity in the room. The AP and the laptop are placed about four metres from each other with a LoS path. By observing the filtered amplitude, we notice significant periodical fluctuations which cause the signal energy to have concentrated at the frequency of below 50 Hz in the spectrogram (Fig. 5 (b), all CSI streams are included) across the duration of the fluctuations. The rest of the spectrogram is clean even with noticeable residual noise after the wavelet filtering. However, the periodical fluctuations make this CSI collection method unsuitable for activity recognition tasks because the frequency of the fluctuations overlaps with the duration of most activity types.

To identify whether this is an AP specific issue, we test the CSI tool with another commercial WiFi AP TPLink AC1200. In Fig. 6 the periodic fluctuations do not appear; however, a significant residual noise remains after the wavelet filtering. In Fig. 6 (b), we can see a significant amount of signal energy at the frequency of below about 70 Hz everywhere across this ten-second section spectrogram, making this AP unsuitable for activity recognition tasks.

It is obvious that there are AP-specific issues while using this CSI collection tool, therefore we test it with another Sagemcom Fast 5364 AC1200 WiFi router. In Fig. 7, we do not observe any major issues that we experienced with the

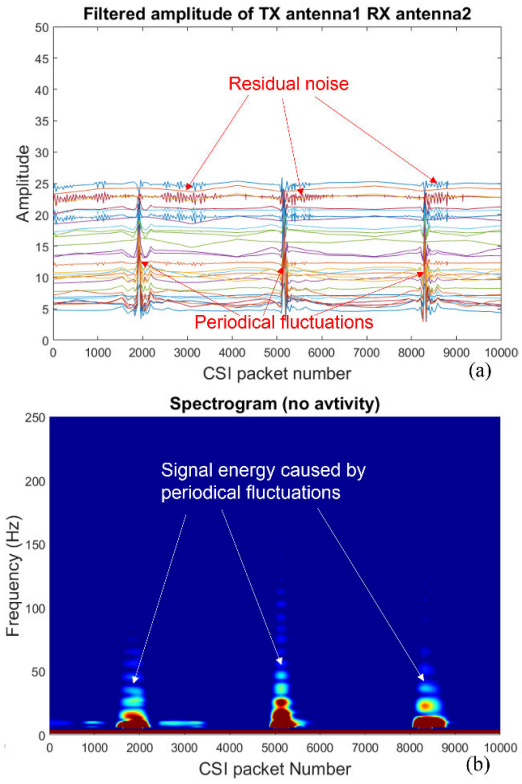

FIGURE 5. (a) Wavelet filtered amplitude of one antenna pair, and (b) Spectrogram, using CSI collected with Netgear WAC104 - AC1200 WiFi AP.

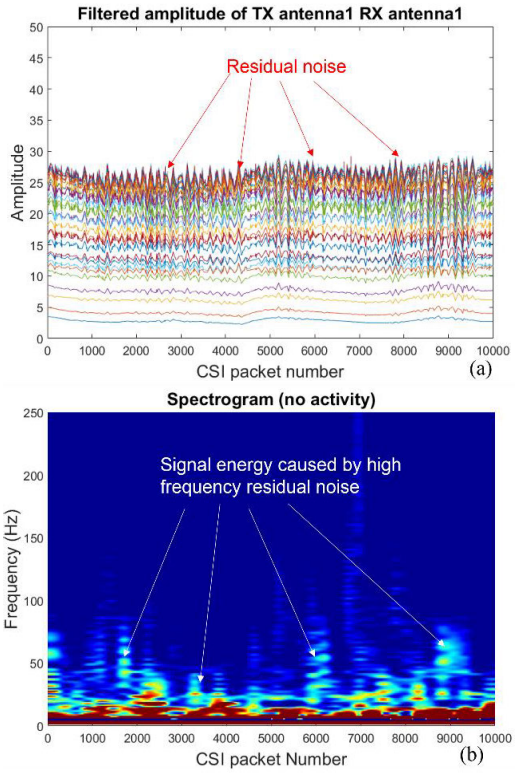

FIGURE 6. (a) Wavelet filtered amplitude of one antenna pair, and (b) Spectrogram, using CSI collected with TP - Link AC1200 WiFi AP.

Netgear and TPLink APs, and the clean spectrogram indicates that this method can be a potential option for the fall detection task.

Fig. 8 presents the spectrograms generated from the CSI collected by the Sagemcom router when there are activities (performed on the LoS path between the laptop and the router) in the room. In Fig. 8 (a), we can observe a consistent signal energy below 50 Hz across the duration of the walking activity and no signal energy outside the activity duration. In Fig. 8 (b), we can see different features between standing up from a chair and sitting down on a chair, as well as some high frequency noise. In terms of the quality of the collected CSI, the CSI tool with Sagemcom router outperforms other APs and this could be suitable for the fall detection task. However, we experience an issue of random WiFi network disconnections during CSI collection which exists across all APs that we tested. To make the laptop re-join the WiFi network the custom firmware of the Intel 5300 NIC needs to be loaded again otherwise the laptop will not join the WiFi network successfully. This issue makes the CSI recording inefficient.

C. CSI COLLECTION USING TWO HOST COMPUTERS WITH INTEL 5300 NIC

The custom firmware for Intel 5300 NIC provided by the Linux CSI tool allows two host computers with Intel 5300 NIC to operate with monitor and injection modes (rather than the typical AP and client modes) specifically for the CSI collection. The computer in injection mode broadcasts CSI packets at a configurable rate on a configurable frequency. The computer in monitor mode passively listens to the CSI packets without having to join a certain WiFi network, which makes this method more reliable than the methods we tested in Subsection II-B) To evaluate this tool we configure the ThinkPad R61 to monitor mode and an Intel NUC D34010WYKH mini-PC to injection mode. With this combination, the collected CSI has three streams from the three RX antennas and one TX antenna.

Fig. 9 depicts the spectrograms of two activities generated from the CSI collected using injection mode. We can clearly observe different signatures of received CSI signal's energy in Fig. 9 (a) when the person bends down to pick up an object on the floor and stands back up, and in Fig. 9 (b) when the person walks in the room and falls onto a mattress. Similar to the spectrograms in Fig. 8, we can see the envelope of the signal energy when there are activities and unwanted low-frequency noise barely exists. During our experiments, the CSI collection experiencing any issues, therefore, in the rest of the paper, we will use the Intel 5300 NIC with injection mode to collect CSI for different activities.

III. DEEP LEARNING BASED FALL DETECTION

Artificial intelligence (AI) has been rapidly developed in recent years and one of its major branches deep neural

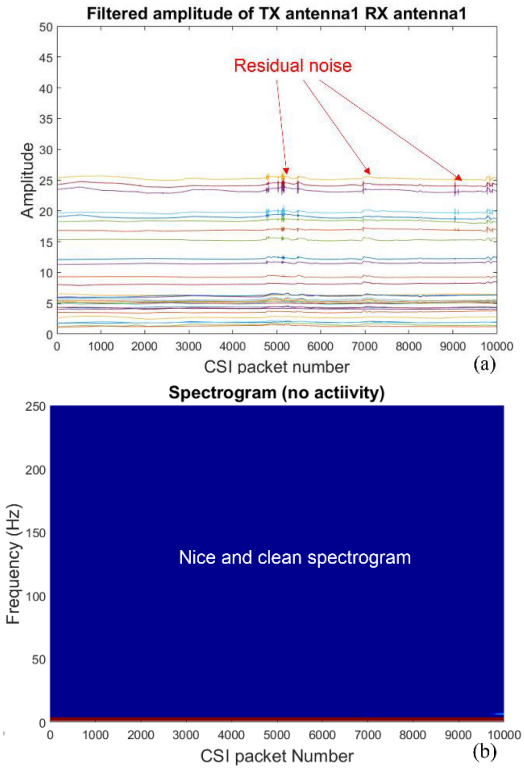

FIGURE 7. (a) Wavelet filtered amplitude of one antenna pair, and (b) Spectrogram, using CSI collected by Sagemcom Fast 5364 AC1200 WiFi router.

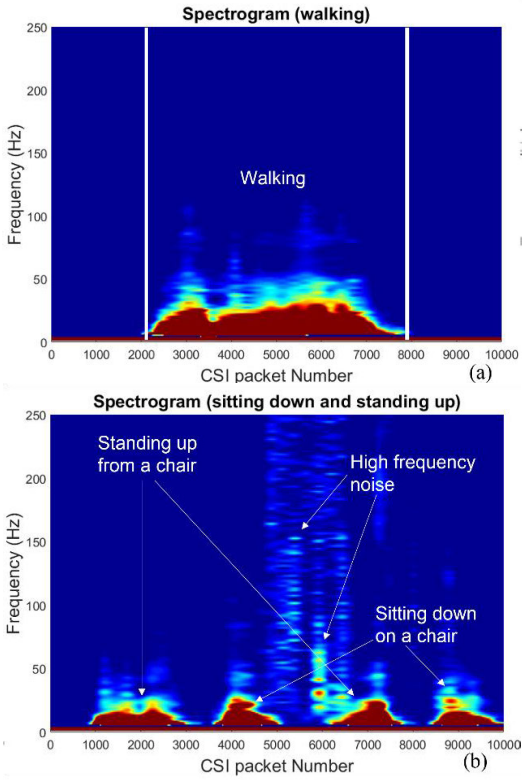

FIGURE 8. Spectrograms of (a) Walking, and (b) Sitting down and standing up.

network (DNN) can be commonly found in many real-world applications, such as object classification and detection, speech recognition and language translation [38]. In this section, we review the recent developments of deep learning based classification and describe the details of the proposed fall detection technique.

A. BACKGROUND OF DEEP LEARNING BASED CLASSIFICATION

The capability of convolutional neural network (CNN) in vision-based applications has outperformed conventional computer vision methods, particularly for object classification, detection and segmentation. The existing open-source large image datasets such as PASCAL VOC [39], Microsoft COCO [40] and ImageNet [38] allow the CNNs to be trained with millions of images containing daily objects to improve the accuracy of detection. Users can fine-tune the pre-trained state-of-the-art CNN models such as AlexNet [41], ResNet [42], GoogleNet [43], VGG [44] and EfficientNet [28]. For example, CNNs with pre-trained ResNet backbones are used in plant counting from aerial images [45] and industrial chimney identification from remote sensing images [46]. ResNet [47] and VGG [48] backbones are used in the diagnosis of COVID-19 from X-ray images. EfficientNet is selected as the backbone of the proposed fall detection due to its advanced features in number of parameters, convergence speed and accuracy.

B. FALL DETECTION WORKFLOW

The proposed fall detection continuously monitors the collected CSI and detects the fall events when they occur. Fig. 10 shows the workflow. The left-column tasks are CSI collection and pre-processing, and the right-column tasks are activity classification. The pre-processing tasks include:

- CSI collection: as described in Subsection II-C), the CSI collection is conducted by a pair of host computers with Intel 5300 NIC using injection mode at the rate of 1000 samples/sec.
- Segmentation: a sliding window is used to capture five-second segments (5 K samples) of the collected CSI samples and the overlap between two consecutive windows can vary depending on the amount of processing power available. According to our observations, one fall event typically lasts for two to four seconds, therefore we choose the five-second sliding window to make sure the fall event is fully covered.
- Denoising: there is an optional denoising step following the sliding window segmentation which uses the same wavelet filter in FallDeFi to reduce the noise of the CSI. The effect of the denoising step will be investigated in Section V.
- Down sampling: the sample segment is down sampled by a factor of 8 to reduce the size of the segment to 625 samples. Given the original 1 kHz sampling rate,

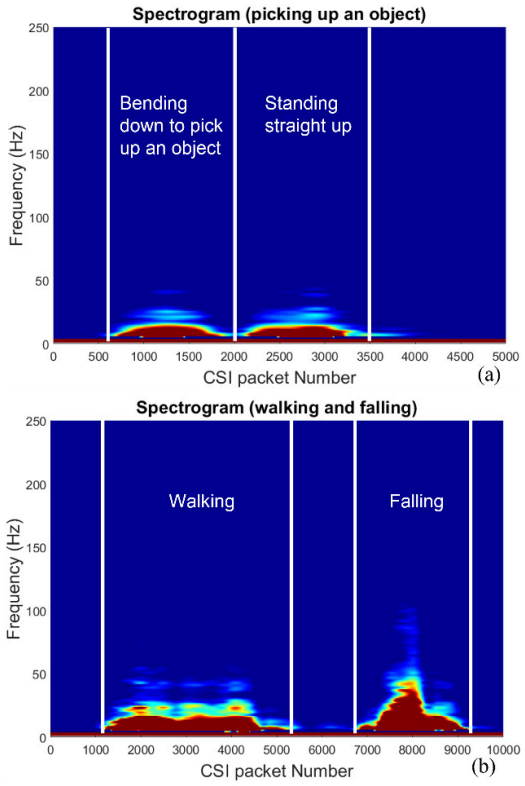

FIGURE 9. Spectrograms of (a) Picking up and object on the floor, and (b) Walking and falling.

the down-sampled segment has an equivalent 125 Hz sampling rate which preserves features below 62.5 Hz. As pointed out in [14], the strongest signal energy of high-frequency activities is concentrated at the Doppler Frequency of below 30 Hz for the 5.2 GHz WiFi signals. Based on our observations even the falls performed on the LoS path between two closely placed host computers (which is the activity containing the most high frequency signal energy), it is unlikely for strong signal energy to appear at the frequency of above 60 Hz. Therefore, the equivalent 125 Hz sampling rate is sufficient to capture features of the target activities. This results in a much smaller sample segment size (625 down from 5 K), which benefits the training and inference time.

- Reshaping and normalisation: the segment is reshaped from a 2-D "image" to a 3-D "image". The segment before reshaping has the size of 625 × 90, which includes 625 CSI samples and 90 CSI streams (one TX antenna and three RX antennas). It is reshaped to the size of 3 × 625 × 30, where the first dimension represents the three channels of RGB images ([38]). Each channel contains the CSI samples collected by the same TX and RX antenna pair. Before the segment is sent to the classifier, the data of three channels is normalised with mean values equal to 0.485, 0.456, and 0.406, and standard deviation equal to 0.229, 0.224, and 0.225 according to the input requirements of EfficientNet. The normalised segment is then sent to the classifier for binary classification to identify whether it contains a fall event or not.

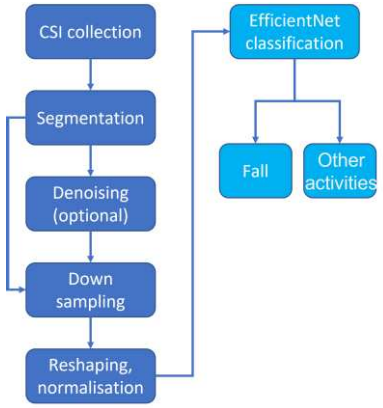

FIGURE 10. Fall detection workflow.

The original EfficientNet is designed to classify the images in the ImageNet dataset, which has 1000 classes. In this paper, we develop a classifier for binary classification based on EfficientNet. Fig. 11 shows the stages of the original EfficientNetB0 [28] with the detailed layers of Stage 9 (which is shared across EfficientNetB0 to B6). We replace the layers after global pooling with three fully connected (FC) layers with SiLU activation function and two dropout layers to make the network suitable for binary classification (rather than the original 1000 classes) and to reduce overfitting. Transfer learning is used for training the modified network by initialising the network with ImageNet pretrained weights.

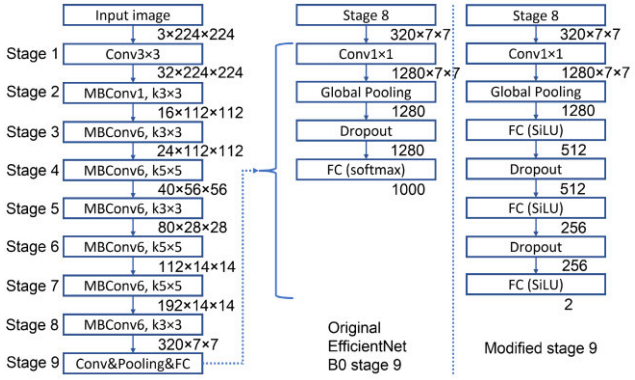

FIGURE 11. Modified EfficientNet B0 [28].

IV. CSI COLLECTION AND DATASET CONSTRUCTION

A comprehensive dataset, which covers various daily activities and assorted WiFi propagation environments, is of paramount importance to develop a reliable fall detection system, which can correctly identify fall events in different environments. In this section, we provide the details of our CSI data collection and dataset construction.

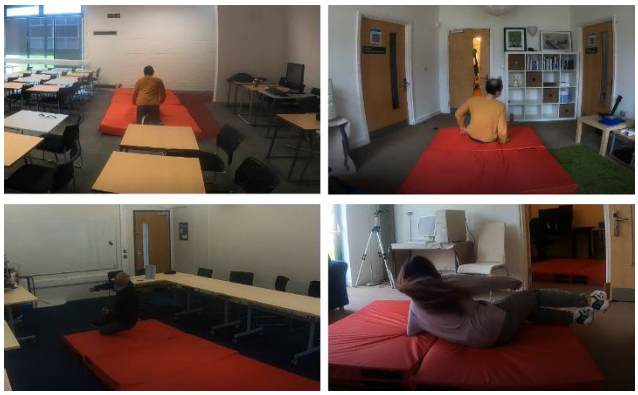

FIGURE 12. Examples of falls during CSI collection.

A. CSI COLLECTION

In order to construct a comprehensive CSI dataset of fall events of different people, we recruited twenty-two volunteers (aged from 24 to 43, 7 females and 15 males) to perform falls and other daily activities. The falls each volunteer performed included falling in to four different directions (front, back, left, and right) onto a mattress. Other than the general fall directions, we asked the volunteers to perform random activities immediately before falls such as standing still, walking forwards, and slowly moving backwards/sideways. For health and safety reasons there were no specific requirements to the velocity or posture of the falls, and the volunteers performed falls with their own comfortable speed. The preferences of the volunteers resulted in various types of falls such as hard falls with limbs and torso touching the mattress almost simultaneously, and less intensive two-step falls with knees/hip first touching the mattress. Fig. 12 shows examples of falls performed by volunteers during the CSI collection. The other daily activities performed included bending down to pick up an object on the ground and standing straight up, sitting down on a mattress (from standing) and standing up from a mattress, walking, and waving both arms while standing and walking. The CSI collected while no activities in the room are also included in the dataset. Fig. 13 compares the spectrograms generated from the CSI collected in the same room while different activities occur. Note that the spectrograms are generated using the original CSI collected at 1 KHz (before the down sampling step) and the maximum frequency of the spectrograms is set to 100 Hz to improve the readability.

Fig. 14 illustrates the floor plans of four different indoor rooms we used to collect CSI. Locations of the WiFi TXs and RXs are marked on the floor plans as well as the locations where the activities are performed. Note that the falls are not performed at all locations for health and safety reasons. Room A (Fig. 14 (a)) is the living room in a residential property. The TX is placed at the top-left corner. About half of the activities are performed while the RX is placed at the RX1 location, and the other half of the activities are performed while the RX is placed at the RX2 location. The RX1 location has NLoS to the TX and the RX2 location has LoS. The RX is about 1 m above the ground at both locations. Falls are performed on the sofa as well as a mattress placed near the sofa. This room has the shortest WiFi propagation distance. Room B (Fig. 14 (b)) is a medium-size meeting room with office desks and chairs. WiFi TX and RX are placed on office desks (about 90 cm in height) at the bottom-left and top-right corners respectively. There is LoS between the two WiFi devices and the activities are performed in the centre area of the room. Environment C (Fig. 14 (c)) is part of the Home Lab (Computer Science, University of York, 2022). The Home Lab includes two living rooms, a kitchen, and an entrance room. The kitchen (not shown on the floor plan) is not used for CSI collection for health and safety concerns. The TX is placed on a chair in the entrance room at a height of about 50 cm above the ground, the RX is placed on a coffee table at a similar height in the left-hand-side living room. Activities are performed in both living rooms as well as some non-fall activities in the entrance room (such as walking). The activities in the left-hand-side living room and the entrance room are on the LoS path but the activities in the right-hand-side living room are off the LoS path. Room D (Fig. 14 (d)) is a large lecture room with office desks and chairs. The TX and RX are placed on two office desks at about 80 cm height. LoS generally exists between the TX and RX, however, there are a few desks and chairs (with metal frames) on the path. Most activities are performed near the TX with some non-fall activities performed in the centre of the room. The positions of some small furniture (such as desks, chairs, and tea tables) are moved across sessions to create a slightly different propagation environment.

B. DATASET PREPARATION

During the CSI data collection, timestamps are included in the CSI files and the activities in the room are recorded with a GoPro camera with timestamp overlay enabled. These timestamps allow the CSI data to be annotated with the correct activities. Every raw CSI file typically contains the CSI collected with a duration of one to two minutes, where the volunteer performs the same activity multiple times. To prepare the dataset, we select the CSI data of five-second duration (which only contains one activity) and label it to fall or non-fall event while comparing the timestamps on the CSI file and the recorded video. Across all CSI data collected in the four environments mentioned in Subsection IV-A, we label 321 fall events and 436 non-fall events. Note that the number of volunteers, who attended the data collection in four rooms are different, therefore the number of CSI samples collected are different. Table 2 shows the numbers of fall and non-fall events collected in five different rooms.

Fig. 15 compares the spectrograms of the same fall to the front activity performed in five rooms. The signal energy in the top three figures is concentrated at the frequency of below 50 Hz. This is due to that the activities are performed on the LoS path or the dominant path (e.g., RX1 in living room A) and the moving human body mass is making a

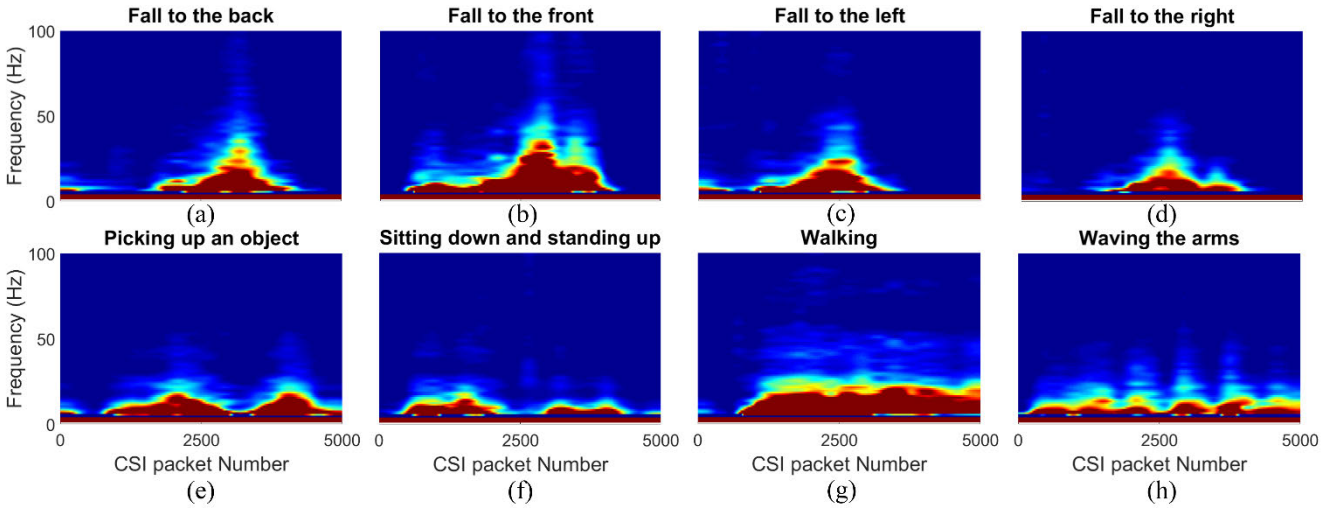

FIGURE 13. Example spectrograms of activities (a) Fall to the back, (b) Fall to the front, (c) Fall to the left, (d) Fall to the right, (e) Bending and picking up an object from the floor and standing straight up, (f) Sitting down and standing up from a mattress, (g) Walking, (h) Waving the arms while standing and walking.

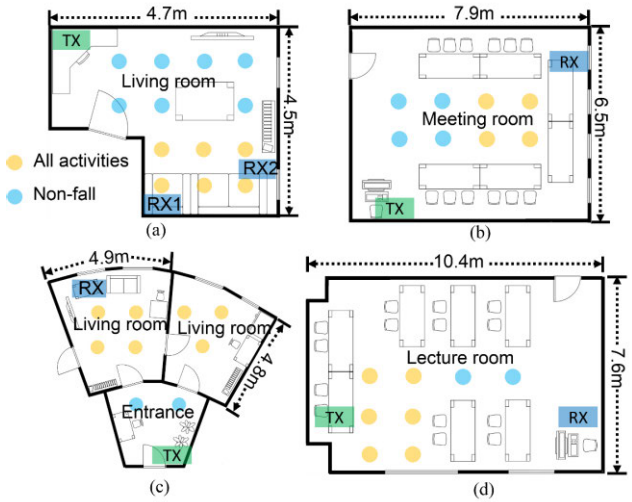

FIGURE 14. Floor plans of the CSI collection environments (a) Living room A, (b) Meeting room B, (c) Home lab C, (d) Lecture room D.

TABLE 2. Number of events collected.

Location	Fall events	Non-fall events	Total
Living room A	91	157	248
Meeting room B	58	76	134
Left living room C	40	45	85
Right living room C	36	49	85
Lecture room D	96	109	205

significant impact to the WiFi signal propagation. However, when the activities are performed on the NLoS path or the non-dominant path (e.g., activities in the right living room in environment C), the high-frequency components of the signal energy are significantly reduced (Fig. 15 (d)), therefore resulting in different features on the spectrograms. Similarly, the signal energy in Fig. 15 (e) has fewer high-frequency components, potentially because of the large propagation distance and the signal path partially obstructed by desks and chairs with metal frames. The high-frequency noise in Fig. 15 (e) appears consistently in the CSI collected in lecture room D and we are unsure of the source of the high frequency noise. There are two CSI collection sessions in this room a week apart and the high frequency noise appears commonly in CSI collected both days regardless of the activities in the room.

The WiFi signal propagation in the four environments mentioned above can all be considered as Rician fading environments where the received signal consists of the signal from a dominant path (mostly a LoS path) and the signals from scattered paths. The Rician faded signal can be expressed as ([49] and [50]):

$$s(t) = k_d cos(\omega_c t + \omega_d t) + \sum_{i=1}^{N} k_{si} cos(\omega_c t + \omega_{d_i} t + \varphi_i) \quad (2)$$

where ω_c is the carrier frequency, k_d is the amplitude of the dominant path component, ω_d is the Doppler shift of the dominant path component, and k_{si}, ω_{d_i} and φ_i are the amplitude, Doppler Shift and phase of the i^{th} scatter component, respectively. The amplitude of $s(t)$ follows Rician distribution with the probability density function (PDF) given by in the following expression [51]:

$$f(x) = \frac{x}{\sigma^2} exp\left(-\frac{x^2 + k_d^2}{2\sigma^2}\right) I_0 \frac{x k_d}{\sigma^2}, \quad (3)$$

where σ^2 is the variance of the signal amplitude x and I_0 is the 0^{th} order modified Bessel function of the first kind. The ratio between the power of the dominant path and the power

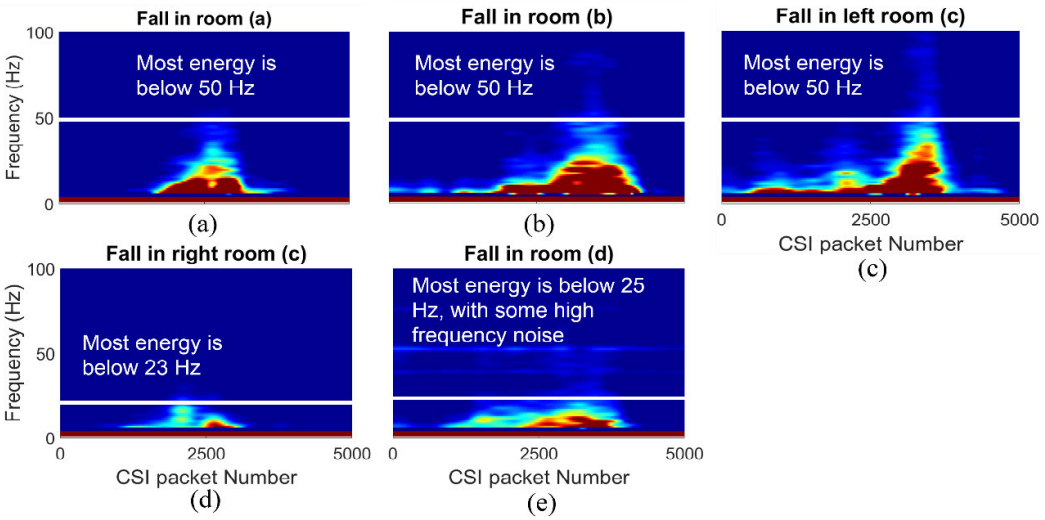

FIGURE 15. Spectrograms of the fall to the front activity in (a) Living room A, (b) Meeting room B, (c) The left-hand-side living room of environment C, (d) The right-hand-side living room of environment C, (e) Lecture room D.

of the scattered paths is described by the K factor, which is given by:

$$K = \frac{k_d^2}{2\sigma^2}. \tag{4}$$

For typical indoor environments the values of the K factor range roughly between 4 dB and 10 dB [52], which means that the dominant component contributes significantly more to the received signal strength. In the case of Fig. 15 (d), the activities only affect a proportion of the scattered components, which are less impactful to the overall received signal, therefore resulting in signal energy at lower frequencies on the spectrogram. The differences across the spectrograms of the same activity performed in different rooms also indicate the importance of the diversity of the environments that the dataset includes. For ML based classifiers, the CSI data in Fig. 15 (d) and (e) could easily result in false negatives if the features are not included in the training dataset. On the other hand, if the classifiers are only trained with the CSI data in Fig. 15 (d) and (e), the inference could result in false positives, while predicting the falls in the other three rooms.

V. PERFORMANCE RESULTS AND DISCUSSIONS

In this section, we evaluate performance of the proposed fall detection technique by drawing a performance comparison with the existing two fall detection techniques while including different sets of CSI data collected in the four environments mentioned in Section IV during training. The performance is compared with FallDeFi [14], which uses an SVM-based classifier and the work in [25], which uses a ResNet-based classifier.

A. PERFORMANCE METRICS

The metrics that are used to evaluate the fall detection performance include accuracy, precision and recall. Accuracy indicates the percentage of correctly classified fall and non-fall events among all events. The accuracy of a fall detection system can be defined as follows:

$$\text{Accuracy} = \frac{\text{TP (True Positive)} + \text{TN(True Negative)}}{\text{TP} + \text{TN} + \text{FP (False Positive)} + \text{FN(False Negative)}}. \tag{5}$$

Precision which shows the percentage of correctly detected fall events among all detected fall events:

$$\text{Precision} = \frac{\text{TP}}{\text{TP} + \text{FP}}. \tag{6}$$

And Recall which indicates the percentage of correctly detected fall events among all fall events in the dataset, can be defined as follows:

$$\text{Recall} = \frac{\text{TP}}{\text{TP} + \text{FN}}. \tag{7}$$

B. PERFORMANCE EVALUATION

During every training, we randomly split 80% of the dataset for training and 20% for validation. Dataset shuffle is enabled for the training set and disabled for the validation set. The training and testing are implemented with Pytorch [53] on a computer with an Nvidia RTX 2070 GPU. We use the Adam optimiser with 0.0001 weight decay. Step learning rate scheduler is used to reduce the learning rate across epochs with the step size set to 10, and gamma set to 0.1. The initial learning rate is set to 0.001, the batch size is set to 50 and the number of epochs is set to 40. With the CSI collected in all the environments, we train a few different configurations of classifiers with variations of EfficientNet (B0 and B1), including the original networks and our proposed networks (with and without denoising).

Table 3 provides the performance metrics of the validation set across different configurations of the classifier. It is also clear from Table 3 that the denoising has minimal impact on the performance of the classifier. Therefore, we will not include denoising in the workflow for the evaluations later. We can also see significant improvements between the original EfficientNet variants and the proposed networks. The data in Table 3 also shows that the modified B0 performs slightly better than the modified B1. We also implemented FallDeFi [14] using the Matlab code[2] shared by the authors and the work proposed in [25] with Pytorch for comparison. The best performance metrics are marked with **bold font**.

TABLE 3. Performance comparison of classifiers trained and tested with entire dataset.

Model	Accuracy	Precision	Recall
Original B0, no denoising	85.7%	79.2%	91.2%
Original B0, denoising	85.9%	81.1%	91.9%
Original B1, no denoising	89.9%	87.3%	88.6%
Original B1, denoising	90.2%	88.1%	89.2%
Modified B0, no denoising	**96.8%**	**96.0%**	**96.9%**
Modified B1, no denoising	96.1%	94.8%	96.3%
FallDefi [14]	82.1%	79.6%	83.5%
Work in [25]	90.8%	89.7%	91.4%

Table 4 compares the performance of the classifiers trained with the entire dataset but evaluated with datasets including combinations of CSI collected in different rooms. From the examples in Fig. 15, we can see similar features from the top three spectrograms, therefore we group the datasets from these three rooms together (living room A, meeting room B and left living room C) for testing. During the CSI collection in these three rooms, the activities are mostly performed on the LoS or dominant path. From the performance metrics in Table 4, we can realise our modified classifiers outperform others in every scenario with the modified B1 slightly outperforms the modified B0. Reduced performance can be clearly observed while testing with the dataset collected in the right living room of environment C. FallDeFi [14] and the work proposed in [25] experience significant reductions with the accuracy dropped to below 76% while our Modified B1 has the accuracy remained over 92%. This could be caused by the relatively small dataset (85 events out of the total 757 events) and the similar features between the falls in this room and some non-fall events in other rooms.

Table 5 presents the effect of different sets of volunteers performing the activities. The activities in the rooms in Fig. 14 (b) and (c) are performed by the same set of seven volunteers. This set of volunteers is the subset of the volunteers (seven out of sixteen), who performed the activities in the room in Fig. 14 (d). The six volunteers that join the CSI collection sessions in the room in Fig. 14 (a) are completely different from the other rooms. Therefore, we group up the CSI collected in the rooms in Fig. 14 (b) and (c) for training then evaluate the performance with the training dataset as well as the datasets collected in two other rooms. We can see that all four classifiers have better performance than Table 3 while testing with the training dataset. A large proportion of false positives (FPs, false alarms) can be observed across all four classifiers while testing with CSI collected in the living room A. This could be caused by the combined effect of different environments and different sets of volunteers. The performance improves while testing with CSI collected in the lecture room D.

Table 6 demonstrates the effect of different environments while the activities are performed by a similar set of volunteers. We combine the CSI collected in meeting room B and lecturer room D as the training dataset (339 samples) and test the performance with the training dataset as well as the datasets collected in the two living rooms of the environment C. In this case the set of volunteers performing activities in the two living rooms of environment C is the subset of the volunteers performing activities in the training dataset. Compared to the results in Table 3, almost all performance metrics of four classifiers are increased when testing with the training dataset. Performance drop across all four classifiers can be observed while testing with the datasets collected in environment C, particularly in the right-hand-side living room. We can see the Accuracy of our modified B1 still remains above 80% while the other classifiers have the Accuracy significantly dropped. We can also see an increasing number of false alarms while testing with the dataset of the right-hand-side living room. This is consistent with the results in Table 4 because the features of the falls performed in this room (off the dominant path, e.g. Fig. 15 (d)) are similar to the features of some non-fall activities performed in other rooms on the dominant paths.

Table 7 compares the complexity and computation time across the proposed work and the works in [14] and [25]. The computation time includes the processing time of a single CSI sample of a 5-second period. The pre-processing time indicates the time consumption for preparing (on CPU) the raw CSI samples for input to the classifier. The inference of the proposed work and the work in [25] was conducted on an Nvidia RTX 2070 GPU, and FallDeFi [14] was conducted on an Intel i7-10750H CPU. The proposed work has negligible pre-processing time because of the minimum pre-processing required before classification (only down sampling). The other two works have significantly longer pre-processing time due to the generation of spectrograms and wavelet denoising. The proposed work also has faster inference time compared to the work in [25], benefiting from less parameters and smaller input size ($3 \times 625 \times 30$ against $3 \times 227 \times 227$). The lower complexity and computation time of the proposed work allow the potential of conducting multiple tasks in parallel with the same hardware.

C. LIMATATIONS AND CHALLENGES

From the performance results presented in Subsection V-B, we can see that the proposed fall detection technique

[2]https://github.com/dmsp123/FallDeFi

TABLE 4. Performance comparison of classifiers trained with the entire dataset and tested with combinations of datasets.

Model	Living room A, meeting room B and left living room C			Right living room C			Lecture room D		
	Accuracy	Precision	Recall	Accuracy	Precision	Recall	Accuracy	Precision	Recall
Modified B0	**97.9%**	**97.3%**	97.2%	82.0%	72.7%	**100.0%**	93.5%	92.5%	94.7%
Modified B1	97.5%	95.5%	**98.0%**	**92.0%**	**90.9%**	90.9%	**95.5%**	**94.7%**	**95.8%**
FallDefi [14]	83.2%	80.9%	84.2%	68.2%	66.4%	70.9%	80.5%	78.2%	81.6%
Work in [25]	91.3%	90.2%	93.5%	75.4%	72.7%	76.2%	85.6%	83.8%	88.9%

TABLE 5. Performance comparison of classifiers trained with the rooms in Fig. 14 (b) and (c) and tested with combinations of datasets.

Model	Meeting room B and both living rooms of environment C			Living room A			Lecture room D		
	Accuracy	Precision	Recall	Accuracy	Precision	Recall	Accuracy	Precision	Recall
Modified B0	98.7%	97.0%	**100.0%**	**69.0%**	**54.6%**	90.0%	72.5%	69.0%	76.5%
Modified B1	**99.0%**	**97.8%**	**100.0%**	67.5%	54.2%	92.2%	**78.5%**	**75.3%**	**80.3%**
FallDefi [14]	89.6%	87.3%	95.1%	59.7%	49.3%	79.4%	68.3%	66.4%	71.6%
Work in [25]	96.3%	93.2%	97.8%	65.9%	53.2%	**93.5%**	73.2%	71.7%	76.9%

TABLE 6. Performance comparison of classifiers trained with the rooms in Fig. 14 (b) and (e) and tested with different datasets.

Model	Meeting room B and lecturer room D			Left living room of environment C			Right living room of environment C		
	Accuracy	Precision	Recall	Accuracy	Precision	Recall	Accuracy	Precision	Recall
Modified B0	**99.0%**	**100.0%**	**98.0%**	**90.0%**	**91.7%**	88.0%	78.0%	65.5%	**95.0%**
Modified B1	97.3%	96.2%	97.2%	84.0%	82.8%	**88.9%**	**80.0%**	**72.4%**	91.3%
FallDefi [14]	86.3%	85.6%	90.4%	72.6%	69.3%	79.5%	68.3%	62.1%	75.6%
Work in [25]	92.7%	91.5%	94.2%	75.7%	74.4%	82.8%	73.2%	68.3%	84.6%

TABLE 7. Complexity and computation time comparison.

Model	Pre-processing time (ms)	Inference time (ms)	Number of parameters
Modified B0	<1	<1	5.3 M
Modified B1	<1	<1	7.8 M
FallDefi [14]	153	1160	n/a
Work in [25]	87	<5	13.6 M

outperforms two other state-of-the-art fall detection systems in all test scenarios. This technique achieves the accuracy of over 97% with LoS and remains over 92% without LoS (results in Table 4). Although the proposed technique advances the state-of-the-art, there are still limitations to be further investigated.

- Activities performed off the dominant or LoS path have significantly different features (much lower frequencies for the same activities) and result in many FPs if not included in the training dataset. As we mentioned in Subsection IV-B, most indoor WiFi propagations follow Rician fading where a large proportion of the received signal contributed by the dominant or LoS path and the activities occur off these paths naturally have reduced impact to the CSI. This is unavoidable in a practical scenario since the falls could happen anywhere in the rooms where the location is accessible, and it is impractical to place many WiFi TXs and RXs to make dominant paths to cover all fall locations. To mitigate this issue, enough samples collected off the dominant paths should be included in the training dataset so the classifiers could recognise the corresponding features.
- Not only the changes in the environment affect the detection accuracy, but also the volunteers who perform the activities. The volunteers contributed to the data collection include both males and females with age from 24 to 43. For health and safety concerns, we do not have specific requirements for the velocity or posture of the falls, and the volunteers performed falls with their own comfortable speed. This results in variants of the same activity across multiple volunteers. The impact of different sets of volunteers can be observed by comparing the data in Tables 4 and 5. The detection accuracy reduction is significant when the environment and volunteer set are both changed. However, the reduction is much less if the activities (collected in different environments) of the volunteers are included in the training dataset. For example, in Table 5, our modified B1 classifier achieves 80% accuracy (right living room of environment C) even when the activities performed off the LoS path are not included in the training dataset, because the activities performed by the same set of volunteers in other environments have been included in the training dataset.
- For health and safety concerns we recruited relatively young volunteers to perform the required activities

which indicates that the activities performed by older people are missing from the dataset. As described by the previous point the activities performed by different people could have significant impact to the detection accuracy, a fall detection system trained based on the dataset including activities performed by younger people may not be as accurate while testing with activities performed by older people. Including activities in different environments performed by different people always help with the applicability of the fall detection system in real world scenarios. Due to the scale of our work, we could only conduct our experiments in a certain number of indoor environments with the support of a reasonable number of volunteers. However, given that our work is available in the public domain, the readers interested in similar applications could easily expand our work to achieve better performance and use our dataset to enhance existing works.

- As mentioned by the previous point, health and safety are one of the major concerns while conducting research involving human subjects. The university has strict requirements on assessing health and safety risks as well as the risk mitigation methods. The activities with moderate to high risks of any injuries are either prohibited or require specific measures to reduce the level of risks. This brings limitations to some activities that are important to real-world applications. For example, the activities are performed by young to middle aged volunteers because the people with older age will have much high risks of injury when performing falls. The falls are cushioned by a large mattress so that the volunteers are unlikely to land outside the mattress even when they fall towards unintended angles. This requires the room to have large enough space to place the mattress without nearby obstacles. In this case some realistic environments (such as bathroom and kitchen) are not included in the data collection because of the lack of space and higher risks of colliding with surrounded obstacles, where these environments are important for the fall detection. The falls from height above the ground level (e.g., on stairs, chairs and beds) are also not included in the data collection due to the higher risks of injury.

D. FUTURE DIRECTIONS

As discussed in subsection V-C, there are still limitations of our work that need to be addressed to make the work applicable in real-world scenarios and to improve the detection performance against real fall events. Below we discuss the future directions for research and the potential of real-world applications.

- The quality and quantity of the training dataset has significant impact to the performance of deep learning based classifications. Samples collected with different variables always contribute to the performance and generality of the model. In the future, we plan to conduct further CSI data collection with different environments (such as bedrooms, kitchens and bathrooms), different volunteer sets, varying WiFi signal propagations (on and off dominant path in particular) and more types of activities. We will also explore the possibility of exploiting both amplitude and phase of the collected CSI data.
- Other than improving the dataset, in the future we will continue explore state-of-the-art deep learning models to improve the detection accuracy. For example, the recently announced deep learning model CoCa [54] has outperformed others on the ImageNet image classification accuracy and CoCa can potentially be adapted to the fall detection tasks. We will also explore fall detection methods beyond WiFi sensing. For example, millimeter-wave radar based fall detection systems [55], [56] which generally offer better LoS detection accuracy than WiFi based fall detection systems due to the natural advantages of higher frequency, with the tradeoff of fall detection capability under NLoS conditions.
- As mentioned in subsection V-C, health and safety requirements have realistic impact to the activities that can be performed as well as the volunteers that can be involved in the data collection. In the future, we plan to further engage with the health and safety experts to assess and mitigate the risks, therefore enhancing the dataset with samples collected from practical scenarios. The detailed activities could involve risk assessment and mitigation when the falls are performed in more challenging environments such as bathrooms and kitchens, the data collection involving volunteers with older age groups, and more challenging types of falls from a non-standing posture (such as falls from a chair while sitting and from a bed while laying down).
- Multiple issues need to be addressed for the WiFi CSI based fall detection to be used in real-world applications. At the moment, although WiFi devices are widely used in homes, the regular WiFi hardware may not be suitable for fall detection. Our experiments in section II show that WiFi devices from different manufacturers have their own features in the collected CSI and not all hardware is suitable for fall detection. The WiFi CSI is not only affected by the propagation environments but also the interference from other sources on the same frequency. How the fall detection coexists with different types of interference needs to be investigated to ensure the accuracy of the detection. In a real-world deployment, any FN or FP should be prevented because of the losses and risks come with them. A second system should present in parallel and external intervention could be implemented (such as activating vision-based monitoring) when the results from two systems differ, and this also minimises the potential interrupt to privacy of the vision-based systems (because they do not need to be always activated). For ease of use in real-world applications, the designed fall detection system needs to be low cost and have the

plug-and-play feature. The system should consist of low-cost hardware and a balanced functional split between distributed and centralised nodes. For example, the CSI collection and pre-processing can be conducted by the distributed nodes in homes and the final inference can be uploaded on centralised computing nodes with GPUs.

VI. CONCLUSION

In this paper, we proposed a deep learning based fall detection system using WiFi CSI. In particular, we developed a deep learning classifier based on a state-of-art image classification tool. The CSI of falls and other daily activities were collected in four different indoor environments performed by twenty-two volunteers to create the comprehensive dataset. The dataset also included activities performed on and off the dominant path to improve the applicability of the fall detection system in different occurrences. The proposed fall detection technique outperforms two other fall detection systems and achieves 99% accuracy with certain combinations of the datasets and remains over 96% accuracy when all collected CSI in different environments is included in the training dataset. Although the proposed fall detection technique is effective with our dataset, it still has several constraints and limitations. We summarised the impacts of wireless propagation environments and the people performing the activities and discussed the potential future directions of this work.

ACKNOWLEDGMENT

The authors would like to thank all the volunteers who contributed to the CSI data collection. They would also like to thank the Department of Computer Science, University of York, who provided access to the home laboratory facilities for CSI data collection. The CSI collection has received ethical approval from the Physical Science Ethics Committee at the University of York and the comprehensive instructions on how and where to perform the activities has been provided to the volunteers.

REFERENCES

[1] Office for National Statistics. *Overview of the U.K. Population: January 2021*. Accessed: May 2022. [Online]. Available: https://www.ons.gov.uk/peoplepopulationandcommunity/populationandmigration/populationestimates/articles/overviewoftheukpopulation/january2021

[2] J. Fleming and C. Brayne, "Inability to get up after falling, subsequent time on floor, and summoning help: Prospective cohort study in people over 90," *BMJ*, vol. 337, Nov. 2008, Art. no. a2227.

[3] L. Z. Rubenstein, "Falls in older people: Epidemiology, risk factors and strategies for prevention," *Age Ageing*, vol. 35, no. 2, pp. ii37–ii41, 2006.

[4] A. Beswick, R. Gooberman-Hill, A. Smith, V. Wylde, and S. Ebrahim, "Maintaining independence in older people," *Rev. Clin. Gerontol.*, vol. 20, no. 2, pp. 128–153, May 2010.

[5] Y. Delahoz and M. Labrador, "Survey on fall detection and fall prevention using wearable and external sensors," *Sensors*, vol. 14, no. 10, pp. 19806–19842, Oct. 2014.

[6] M. Habib, M. Mohktar, S. Kamaruzzaman, K. Lim, T. Pin, and F. Ibrahim, "Smartphone-based solutions for fall detection and prevention: Challenges and open issues," *Sensors*, vol. 14, no. 4, pp. 7181–7208, Apr. 2014.

[7] J. Gutiérrez, V. Rodríguez, and S. Martin, "Comprehensive review of vision-based fall detection systems," *Sensors*, vol. 21, no. 3, p. 947, Feb. 2021.

[8] O. Keskes and R. Noumeir, "Vision-based fall detection using ST-GCN," *IEEE Access*, vol. 9, pp. 28224–28236, 2021.

[9] F. Shu and J. Shu, "An eight-camera fall detection system using human fall pattern recognition via machine learning by a low-cost Android box," *Sci. Rep.*, vol. 11, no. 1, pp. 1–17, Jan. 2021.

[10] M. Youssef, M. Mah, and A. Agrawala, "Challenges: Device-free passive localization for wireless environments," in *Proc. 13th Annu. ACM Int. Conf. Mobile Comput. Netw.*, Sep. 2007, pp. 222–229.

[11] H. Steendam and M. Moeneclaey, "Analysis and optimization of the performance of OFDM on frequency-selective time-selective fading channels," *IEEE Trans. Commun.*, vol. 47, no. 12, pp. 1811–1819, Dec. 1999.

[12] X. Liu, J. Cao, S. Tang, J. Wen, and P. Guo, "Contactless respiration monitoring via off-the-shelf WiFi devices," *IEEE Trans. Mobile Comput.*, vol. 15, no. 10, pp. 2466–2479, Oct. 2016.

[13] T. H. Nguyen and H. H. Nguyen, "Towards a robust WiFi-based fall detection with adversarial data augmentation," in *Proc. 54th Annu. Conf. Inf. Sci. Syst. (CISS)*, Mar. 2020, pp. 1–6.

[14] S. Palipana, D. Rojas, P. Agrawal, and D. Pesch, "FallDeFi: Ubiquitous fall detection using commodity Wi-Fi devices," *Proc. ACM Interact., Mobile, Wearable Ubiquitous Technol.*, vol. 1, no. 4, pp. 1–25, Jan. 2018.

[15] N. Damodaran, E. Haruni, M. Kokhkharova, and J. Schäfer, "Device free human activity and fall recognition using WiFi channel state information (CSI)," *CCF Trans. Pervasive Comput. Interact.*, vol. 2, no. 1, pp. 1–17, Mar. 2020.

[16] S. Yousefi, H. Narui, S. Dayal, S. Ermon, and S. Valaee, "A survey on behavior recognition using WiFi channel state information," *IEEE Commun. Mag.*, vol. 55, no. 10, pp. 98–104, Oct. 2017.

[17] H. Wang, D. Zhang, Y. Wang, J. Ma, Y. Wang, and S. Li, "RT-fall: A real-time and contactless fall detection system with commodity WiFi devices," *IEEE Trans. Mobile Comput.*, vol. 16, no. 2, pp. 511–526, Feb. 2017.

[18] L. I. Smith, "A tutorial on principal components analysis," Dept. Comput. Sci., Univ. Otago, Dunedin, New Zealand, Tech. Rep. OUCS-2002-12, 2002.

[19] C. Xu, W. Wang, Y. Zhang, J. Qin, S. Yu, and Y. Zhang, "An indoor localization system using residual learning with channel state information," *Entropy*, vol. 23, no. 5, p. 574, May 2021.

[20] Z. Chen, L. Zhang, C. Jiang, Z. Cao, and W. Cui, "WiFi CSI based passive human activity recognition using attention based BLSTM," *IEEE Trans. Mobile Comput.*, vol. 18, no. 11, pp. 2714–2724, Nov. 2019.

[21] F. Wang, J. Feng, Y. Zhao, X. Zhang, S. Zhang, and J. Han, "Joint activity recognition and indoor localization with WiFi fingerprints," *IEEE Access*, vol. 7, pp. 80058–80068, 2019.

[22] R. Alazrai, M. Hababeh, B. A. Alsaify, M. Z. Ali, and M. I. Daoud, "An end-to-end deep learning framework for recognizing human-to-human interactions using Wi-Fi signals," *IEEE Access*, vol. 8, pp. 197695–197710, 2020.

[23] W. Li, M. J. Bocus, C. Tang, S. Vishwakarma, R. J. Piechocki, K. Woodbridge, and K. Chetty, "A taxonomy of WiFi sensing: CSI vs passive WiFi radar," in *Proc. IEEE Globecom Workshops (GC Wkshps*, Dec. 2020, pp. 1–6.

[24] Y. Wang, K. Wu, and L. M. Ni, "WiFall: Device-free fall detection by wireless networks," *IEEE Trans. Mobile Comput.*, vol. 16, no. 2, pp. 581–594, Feb. 2017.

[25] T. Nakamura, M. Bouazizi, K. Yamamoto, and T. Ohtsuki, "Wi-Fi-CSI-based fall detection by spectrogram analysis with CNN," in *Proc. IEEE Global Commun. Conf. (GLOBECOM)*, Dec. 2020, pp. 1–6.

[26] G. Mattela, M. Tripathi, and C. Pal, "A novel approach in WiFi CSI-based fall detection," *Social Netw. Comput. Sci.*, vol. 3, no. 3, pp. 1–12, May 2022.

[27] Y. Hu, F. Zhang, C. Wu, B. Wang, and K. J. R. Liu, "DeFall: Environment-independent passive fall detection using WiFi," *IEEE Internet Things J.*, vol. 9, no. 11, pp. 8515–8530, Jun. 2022.

[28] M. Tan and Q. Le, "EfficientNet: Rethinking model scaling for convolutional neural networks," in *Proc. Int. Conf. Mach. Learn.*, 2019, pp. 6105–6114.

[29] E. Perahia, "IEEE 802.11n development: History, process, and technology," *IEEE Commun. Mag.*, vol. 46, no. 7, pp. 48–55, Jul. 2008.

[30] D. Halperin, W. Hu, A. Sheth, and D. Wetherall, "Tool release: Gathering 802.11n traces with channel state information," *ACM SIGCOMM Comput. Commun. Rev.*, vol. 41, no. 1, p. 53, Jan. 2011.

[31] Y. Xie, Z. Li, and M. Li, "Precise power delay profiling with commodity WiFi," in *Proc. 21st Annu. Int. Conf. Mobile Comput. Netw.*, Sep. 2015, pp. 53–64.

[32] Espressif. *ESP32*. Accessed: May 2022. [Online]. Available: https://espressif.com/en/products/socs/esp32

[33] S. M. Hernandez and E. Bulut, "Lightweight and standalone IoT based WiFi sensing for active repositioning and mobility," in *Proc. IEEE 21st Int. Symp. World Wireless, Mobile Multimedia Netw. (WoWMoM)*, Aug. 2020, pp. 277–286.

[34] M. Atif, S. Muralidharan, H. Ko, and B. Yoo, "Wi-ESP—A tool for CSI-based device-free Wi-Fi sensing (DFWS)," *J. Comput. Des. Eng.*, vol. 7, no. 5, pp. 644–656, Oct. 2020.

[35] F. Gringoli, M. Schulz, J. Link, and M. Hollick, "Free your CSI: A channel state information extraction platform for modern Wi-Fi chipsets," in *Proc. 13th Int. Workshop Wireless Netw. Testbeds, Exp. Eval. Characterization*, Oct. 2019, pp. 21–28.

[36] Lilygo. *TTGO T8 ESP32-S2 V1.1 WIFI Wireless Module*. Accessed: May 2022. [Online]. Available: http://www.lilygo.cn/prod_view.aspx?TypeId=50063&Id=1300&FId=t3:50063:3

[37] A. J. van den Kroonenberg, W. C. Hayes, and T. A. Mcmahon, "Hip impact velocities and body configurations for voluntary falls from standing height," *J. Biomechanics*, vol. 29, no. 6, pp. 807–811, Jun. 1996.

[38] J. Deng, W. Dong, R. Socher, L.-J. Li, K. Li, and L. Fei-Fei, "ImageNet: A large-scale hierarchical image database," in *Proc. IEEE Conf. Comput. Vis. Pattern Recognit.*, Jun. 2009, pp. 248–255.

[39] M. Everingham, S. M. A. Eslami, L. Van Gool, C. K. I. Williams, J. Winn, and A. Zisserman, "The PASCAL visual object classes challenge: A retrospective," *Int. J. Comput. Vis.*, vol. 111, no. 1, pp. 98–136, Jan. 2015.

[40] T.-Y. Lin, M. Maire, S. Belongie, J. Hays, P. Perona, D. Ramanan, P. Dollár, and C. L. Zitnick, "Microsoft COCO: Common objects in context," in *Proc. Eur. Conf. Comput. Vis.* Cham, Switzerland: Springer, 2014, pp. 740–755.

[41] A. Krizhevsky, I. Sutskever, and G. E. Hinton, "ImageNet classification with deep convolutional neural networks," *Commun. ACM*, vol. 60, no. 6, pp. 84–90, May 2017.

[42] K. He, X. Zhang, S. Ren, and J. Sun, "Deep residual learning for image recognition," in *Proc. IEEE Conf. Comput. Vis. Pattern Recognit. (CVPR)*, Jun. 2016, pp. 770–778.

[43] C. Szegedy, W. Liu, Y. Jia, P. Sermanet, S. Reed, D. Anguelov, D. Erhan, V. Vanhoucke, and A. Rabinovich, "Going deeper with convolutions," in *Proc. IEEE Conf. Comput. Vis. Pattern Recognit. (CVPR)*, Jun. 2015, pp. 1–9.

[44] K. Simonyan and A. Zisserman, "Very deep convolutional networks for large-scale image recognition," 2014, *arXiv:1409.1556*.

[45] M. Machefer, F. Lemarchand, V. Bonnefond, A. Hitchins, and P. Sidiropoulos, "Mask R-CNN refitting strategy for plant counting and sizing in UAV imagery," *Remote Sens.*, vol. 12, no. 18, p. 3015, Sep. 2020.

[46] C. Han, G. Li, Y. Ding, F. Yan, and L. Bai, "Chimney detection based on faster R-CNN and spatial analysis methods in high resolution remote sensing images," *Sensors*, vol. 20, no. 16, p. 4353, Aug. 2020.

[47] S. Hira, A. Bai, and S. Hira, "An automatic approach based on CNN architecture to detect COVID-19 disease from chest X-ray images," *Appl. Intell.*, vol. 51, no. 5, pp. 2864–2889, May 2021.

[48] M. S. Al-Rakhami, M. M. Islam, M. Z. Islam, A. Asraf, A. H. Sodhro, and W. Ding, "Diagnosis of COVID-19 from X-rays using combined CNN-RNN architecture with transfer learning," *BenchCouncil Trans. Benchmarks, Standards Eval.*, vol. 2, no. 4, p. 100088, 2022.

[49] A. Doukas and G. Kalivas, "Rician K factor estimation for wireless communication systems," in *Proc. Int. Conf. Wireless Mobile Commun. (ICWMC)*, Jul. 2006, p. 69.

[50] S. Kumar, P. K. Gupta, G. Singh, and D. S. Chauhan, "Performance analysis of Rayleigh and Rician fading channel models using MATLAB simulation," *Int. J. Intell. Syst. Appl.*, vol. 5, no. 9, pp. 94–102, Aug. 2013.

[51] A. Papoulis and S. U. Pillai, *Probability, Random Variables, and Stochastic Processes*. New York, NY, USA: McGraw-Hill, 2002.

[52] S. Mukherjee, S. S. Das, A. Chatterjee, and S. Chatterjee, "Analytical calculation of Rician K-factor for indoor wireless channel models," *IEEE Access*, vol. 5, pp. 19194–19212, 2017.

[53] A. Paszke et al., "PyTorch: An imperative style, high-performance deep learning library," in *Proc. Adv. Neural Inf. Process. Syst.*, vol. 32, 2019, pp. 1–12.

[54] J. Yu, Z. Wang, V. Vasudevan, L. Yeung, M. Seyedhosseini, and Y. Wu, "CoCa: Contrastive captioners are image-text foundation models," 2022, *arXiv:2205.01917*.

[55] C. Yu, Z. Xu, K. Yan, Y.-R. Chien, S.-H. Fang, and H.-C. Wu, "Noninvasive human activity recognition using millimeter-wave radar," *IEEE Syst. J.*, vol. 16, no. 2, pp. 3036–3047, Jun. 2022.

[56] B. Wang, Z. Zheng, and Y.-X. Guo, "Millimeter-wave frequency modulated continuous wave radar-based soft fall detection using pattern contour-confined Doppler-time maps," *IEEE Sensors J.*, vol. 22, no. 10, pp. 9824–9831, May 2022.

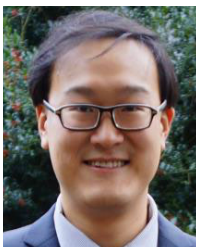

YI CHU received the B.Sc. degree in electronic engineering from China Agriculture University, Beijing, China, in 2008, and the M.Sc. degree in communications engineering and the Ph.D. degree in electronic engineering from the University of York, in 2009 and 2014, respectively. He was a Research Associate with the Center for High Altitude Platform Applications (CHAPA), University of York. He is currently a Research Fellow with the Institute for Safe Autonomy (ISA), School of Physics, Engineering and Technology, University of York. His research interests include wireless and quantum communications applications on aerial platforms, private 5G network deployments, open-RAN network implementation, communications system evaluation using software-defined radio, multi-element antenna array, wireless signal propagation, physical layer network coding, and intelligent medium access control for wireless sensor networks.

KANAPATHIPPILLAI CUMANAN (Senior Member, IEEE) received the B.Sc. degree (Hons.) in electrical and electronic engineering from the University of Peradeniya, Sri Lanka, in 2006, and the Ph.D. degree in signal processing for wireless communications from Loughborough University, Loughborough, U.K., in 2009. From January 2006 to August 2006, he was a Teaching Assistant with the Department of Electrical and Electronic Engineering, University of Peradeniya. In 2011, he was an Academic Visitor with the Department of Electrical and Computer Engineering, National University of Singapore, Singapore. From March 2012 to November 2014, he was a Research Associate with the School of Electrical and Electronic Engineering, Newcastle University, Newcastle upon Tyne, U.K. Prior to this, he was with the School of Electronic, Electrical and System Engineering, Loughborough University. He is currently a Senior Lecturer with the Department of Electronic Engineering, University of York, York, U.K. He has authored or coauthored more than 100 journal articles and conference papers which attracted more than 2900 Google scholar citations. His research interests include non-orthogonal multiple access (NOMA), cell-free massive MIMO, physical layer security, cognitive radio networks, convex optimization techniques, and resource allocation techniques. He was a recipient of an Overseas Research Student Award Scheme (ORSAS) from Cardiff University, Wales, U.K., where he was a Research Student, from September 2006 to July 2007. He is currently an Associate Editor of IEEE JOURNAL OF SELECTED AREAS IN COMMUNICATIONS (JSAC)-MACHINE LEARNING IN COMMUNICATIONS AND NETWORKS, IEEE WIRELESS COMMUNICATIONS LETTERS, and IEEE OPEN JOURNAL OF COMMUNICATIONS SOCIETY.

SATHISH K. SANKARPANDI received the bachelors's engineering degree (B.Tech) from VIT University, India, in 2010, and the Ph.D. degree from Newcastle University, U.K., in 2014. He currently serves as the CTO of VirtTuri Ltd (https://virtturi.com/), a cutting-edge clinical informatics avatar aimed at reducing inequalities and enhancing healthcare outcomes. He leads a highly skilled team that challenges the frontiers of AI and ML. With over a decade of experience, he has successfully completed numerous challenging and innovative data science projects for both the public and private sectors. His doctoral research focused on ''Elderly Falls Prediction using Wearable Sensors,'' employing machine learning techniques. His interests encompass AI and machine learning, the development of predictive models, Natural Language Processing (NLP), prediction science utilising wearable sensor data, as well as the development and commercialization of AI products.

STEPHEN SMITH (Member, IEEE) received the B.Sc. degree in computer science and the M.Sc. and Ph.D. degrees in the application of computational intelligence to problems in healthcare, with a focus on an objective assessment of neurological conditions. He is currently a Professor of electronic engineering with the School of Physics, Engineering and Technology, University of York, U.K. Whilst engaged as a Royal Academy of Engineering Enterprise Fellow, he co-founded the university spinout company ClearSky Medical Diagnostics Ltd. (www.clearskymd.com) which develops and markets intelligent medical devices to assist diagnosis and monitoring of Parkinson's, Alzheimer's, and related neurodegenerative conditions. He is a Chartered Engineer and a fellow of BCS.

OCTAVIA A. DOBRE (Fellow, IEEE) received the Dipl.-Ing. and Ph.D. degrees from the Polytechnic Institute of Bucharest, Romania, in 1991 and 2000, respectively. From 2002 and 2005, she was with the New Jersey Institute of Technology, USA. In 2005, she joined Memorial University, Canada, where she is currently a Professor and the Canada Research Chair Tier 1. She was also a Visiting Professor with the Massachusetts Institute of Technology, USA, and Université de Bretagne Occidentale, France. Her research interests include wireless communication, networking technologies, and optical and underwater communications. She has coauthored more than 450 refereed articles in these areas. She is an Elected Member of the European Academy of Sciences and Arts, a fellow of the Engineering Institute of Canada, and a fellow of the Canadian Academy of Engineering. She serves as the Director of Journals of the Communications Society. She was the inaugural Editor-in-Chief (EiC) of the IEEE Open Journal of the Communications Society and the IEEE Communications Letters. She served as the general chair, the technical program co-chair, the tutorial co-chair, and the technical co-chair of symposia at numerous conferences. She was a Fulbright Scholar, Royal Society Scholar, and Distinguished Lecturer of the IEEE Communications Society. She received the Best Paper Awards at various conferences, including IEEE ICC, IEEE GLOBECOM, IEEE WCNC, and IEEE PIMRC.